Alternate Anodes for the Electrolytic Reduction of UO_2

AUGUSTUS MERWIN and DEV CHIDAMBARAM

The electrolytic reduction process of UO_2 employs a platinum anode and a stainless steel cathode in molten LiCl-LiO_2 maintained at 973 K (700 °C). The degradation of platinum under the severely oxidizing conditions encountered during the process is an issue of concern. In this study, Inconel 600 and 718, stainless steel alloy 316, tungsten, nickel, molybdenum, and titanium, were investigated though electrochemical polarization techniques, electron microscopy, Raman spectroscopy, and X-ray photoelectron spectroscopy to serve as potential anode materials. Of the various materials investigated, only tungsten exhibited sufficient stability at the required potential in the molten electrolyte. Tungsten anodes were further studied in molten LiCl-LiO_2 electrolyte containing 2, 4, and 6 wt pct of Li_2O. In LiCl-2 wt pct Li_2O tungsten was found to be sufficiently stable to both oxidation and microstructural changes and the stability is attributed to the formation of a lithium-intercalated tungsten oxide surface film. Increase in the concentration of Li_2O was found to lead to accelerated corrosion of the anode, in conjunction with the formation of a peroxotungstate oxide film.

DOI: 10.1007/s11661-014-2633-2

I. INTRODUCTION

A key component in the Integral Fast Reactor fuel cycle is the electrometallurgical reprocessing process, also known as pyroprocessing, developed at Argonne National Laboratories.[1,2] Pyroprocessing offers numerous advantages over PUREX and other conventional aqueous reprocessing methods of which most notable are proliferation resistance and increased separation efficiency of actinides.[3,4] Current supplies of UO_2 need to be reduced to metallic uranium before they can be pyroprocessed. An electrolytic reduction process for UO_2 in molten salt has been developed and successfully demonstrated by multiple research groups.[5–11] The current process utilizes platinum as the working anode and a SS 316 basket that contains the UO_2, as cathode.[6] Platinum undergoes corrosion in this electrolyte system and thus there is a need to investigate alternative anode materials that can maintain their stability for a significant amount of time before replacement is essential.

The electrochemical half-cell reactions and standard cell potential of the electrolytic reduction process under standard conditions in LiCl at 923 K (650 °C) were calculated using thermochemical software by researchers at Idaho National Laboratories and Park *et al.*,[6,12] the results of which are summarized below.

AUGUSTUS MERWIN, Doctoral Student, and DEV CHIDAMBARAM, Professor, are with Materials Science and Engineering, University of Nevada, Reno, 1664 N. Virginia St. MS 0388, Reno, NV 89557-0388. Contact e-mail: dcc@unr.edu
Manuscript submitted May 28, 2014.
Article published online November 12, 2014

Reduction: $UO_2 + 4e^- \rightarrow U_{(m)} + 2O^{2-}$
Oxidation: $2O^{2-} \rightarrow O_{2(g)} + 4e^-$
Cell: $UO_2 \rightarrow U_{(m)} + O_{2(g)}$ $E_o = -2.396V$ *vs* SHE [6, 12]

The electrolyte used in this process is a mixture of LiCl and Li_2O in a temperature range of 923 K to 1023 K (650 °C to 750 °C) with the concentration of Li_2O varying up to its solubility limit of 8.8 wt pct.[5,13,14] In the LiCl-Li_2O electrolyte, additional oxidation reactions include: $2\ Cl^- \rightarrow Cl_2 + 2\ e^-$ and the oxidation of the anode. In these highly oxidizing conditions at the required anodic potential, corrosion of the anode material emerges as a technical challenge.[15]

Platinum has been shown to be susceptible to lithium attack, anodic dissolution and is known to form oxide compounds such as Li_2PtO_3 when anodically polarized in a LiCl-Li_2O electrolyte.[16–22] The consumption and degradation of the platinum anode is not desirable, as it decreases the economic viability of the process and could potentially lead to the failure of the electrolysis circuit by breaking electrical contact between the external power supply and the salt electrolyte.

Recent research has also shown that underpotential deposition of Li on the cathode could assist the kinetics of UO_2 reduction; however, this leads to higher current densities at both electrodes.[19] Furthermore, as soluble fission products accumulate in the salt, the rate of UO_2 reduction has been shown to decrease, resulting in longer electrolysis times.[9] Since Pt is known to oxidize under anodic polarization in the electrolyte, increased current density and longer electrolysis times lead to accelerated degradation of the anode. Considering these facts, and the cost of platinum, it is desirable to find an alternative anode material for this process. Boron-doped diamond has recently been shown to be a viable alternative anode material; however, these anodes are

limited by a minimal anode to cathode surface area ratio and operating temperature.[15]

This study explored the use of various alternative anode materials for the electrolytic reduction of UO_2. When considering the application of a working anode in an electrolytic process, it is important to identify a material that undergoes uniform corrosion as opposed to localized degradation. This is critical for electrodes used in molten salt processes containing oxides, as the environment is highly oxidizing and the identification of an inert material is unlikely.

Accelerated electrochemical tests were performed to study the corrosion rate of the potential anode materials. Subsequent tests evaluated the corrosion resistance and microstructural stability of the material in the LiCl electrolyte at the required anodic potential. During commercial operation of the electrolytic reduction process, the O^{2-} ion concentration will inevitably change due to the imperfect evolution of O_2 gas. Therefore, to investigate the oxidation reactions that will occur during the electrolytic reduction process, potential anode materials were polarized at +2.5 V *vs* SS 316 in a two-electrode setup. The electrolyte consisted of LiCl with varying concentrations of Li_2O.

II. MATERIALS

The composition of the various alloys investigated is shown in Table I. The purity of all metals was greater than 99 wt pct. All alloys were mill-annealed, while metals were studied as drawn. Electrodes were polished using 400 and 600 grit sandpaper successively, followed by a rinse with acetone prior to exposure of the electrolyte. Electrodes were purposely not polished to a mirror finish to simulate real-world conditions. All electrode metals and alloys were purchased from Goodfellow Corporation.

Reagent grade anhydrous LiCl and Li_2O were procured from VWR Scientific. The salts were packed in an argon atmosphere and maintained in a controlled nitrogen environment with <10 ppm O_2 and <1 ppm H_2O and used as such.

III. EXPERIMENTAL

The salt melt was contained in a 4.13-cm ID high-purity graphite crucible inside a glove box. 50 g of LiCl containing 2 to 6 wt pct Li_2O was heated to 973 K (700 °C) and maintained at temperature for 30 minutes prior to the initiation of each experiment. Polarization experiments were conducted in LiCl-2 wt pct Li_2O. Additionally, for reasons discussed in the following section, polarizations of tungsten were conducted in LiCl containing 4 wt pct and 6 wt pct Li_2O. All experiments were conducted at 973 K (700 °C). Electrodes were separated by 1 cm in a triangular symmetry and placed with sufficient accuracy to ensure a temperature uncertainty of less than ±5 °C. The atmosphere in the glove box was maintained using N_2 with less than 10 ppm O_2 and 1 ppm H_2O. The 1-mm diameter electrodes were submerged to a depth of 1cm resulting in a total exposed surface area of 32.2 mm^2. Fresh salt was used in every experiment to minimize corrosion product contamination in the salt and to maintain consistent redox potential between subsequent experiments.

The temperature distribution of the salt melt was determined using an insulated thermocouple. Temperature measurements were made at various electrode positions, and the temperature gradient was found to be ±5 °C along the length of the electrode.

A Gamry® PC4 potentiostat was used to conduct electrochemical experiments. The electrodes were lowered into the salt via an externally controlled automated translation stage to ensure repeatability between experiments. Electrodes were exposed to the molten salt for 30 seconds prior to recording the open circuit potential (E_{OCP}) for 30 seconds and subsequently polarized. Materials were potentiodynamically polarized from −0.4 to +1.5 V *vs* E_{OCP} against a Hastelloy B-3 reference at a scan rate of 1 mV/s to determine the electrochemical potential and passivation characteristics of each material. The corrosion potential (E_{corr}) values reported in the following discussions are the potentials at which the smallest magnitude of current was recorded between the cathodic and anodic regions of the polarization scans. Hastelloy B-3 was employed in the manner of a quasi- or pseudo-reference electrode by exposing a polished wire directly to the electrolyte. The use of such an electrode system does not qualify as a conventional reference electrode as it is not a reversible redox couple; however, the quasi-reference configuration is frequently utilized in electrochemical studies in molten salt due to the inability of any material to act as a perfect reference electrode.[23–25] Usually Ni, W, or Pt is utilized as a quasi-reference electrode; however, the use of one of these materials as a quasi-reference electrode was undesirable as this study investigated Ni, W, and Pt as working electrodes. To maintain the same reference electrode for all tested materials and avoid the use of different reference electrodes based on the material under study, it was necessary to utilize a material that was not being considered as a candidate

Table I. The Composition of the Alloy Metals Studied in Weight Percent as Provided by the Supplier

	Fe wt pct	Cr wt pct	Ni wt pct	Mo wt pct	Alloying Elements
Inconel 600	8	15.5	72	—	Mn/Si/Co
Inconel 718	19	19	53	—	Nb/Mo/Ti
SS 316	balance	18	10	3	Mn
Hastelloy B-3	1.5	1.5	65	28.5	—

anode material. Thus, Hastelloy B-3 was chosen as a quasi-reference. To study the oxidation processes that would occur under highly anodic polarization, a two-electrode configuration was used to subject materials to constant potential polarizations, analogous to the conditions encountered in the electrolytic reduction of UO_2. For reasons described earlier, electrodes were polarized at +2.5 V *vs* SS316 for 10 minutes. All experiments were conducted in duplicates.

Following polarization, electrodes were rinsed with distilled water and acetone before the electrode surface morphology was studied using a Hitachi S-4700 field emission scanning electron microscope (SEM). A Thermo-Scientific DXR dispersive Raman microscope was used to analyze the electrode surface. For Raman analysis, electrodes were hermetically sealed in plastic bags to avoid degradation of hygroscopic surface films. The DXR used a 532-nm wavelength laser at 10 mW with 15 seconds exposures and averaged 64 exposures per spectra. Spectra were recorded across a 300 μm by 300 μm square area and averaged to produce accurate representations of the surface chemistry.

Electrode surfaces were also analyzed using a PHI 5600 X-ray photoelectron spectrometer (XPS). Electrodes were transferred into the spectrometer from the experimental glove box via a sealed transfer vessel to avoid exposure to atmosphere. Monochromatic Al X-ray radiation was used at an accelerating voltage of 14 kV at 350 W, with an 800 μm spot size. Spectra were internally calibrated to the adventitious C 1s peak at 284.6 eV.

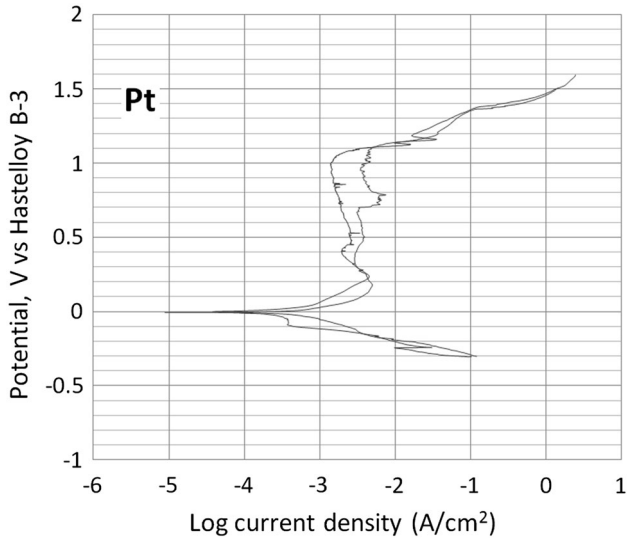

Fig. 1—Potentiodynamic polarization scans of Pt obtained against a Hastelloy B-3 reference in LiCl-2 wt pct Li_2O at 973 K (700 °C). The scans were performed at a rate of 1 mV/s. Duplicate scans are shown.

IV. RESULTS AND DISCUSSION

In order to establish a benchmark comparison, experiments were conducted using Pt. The potentiodynamic polarization data for Pt against a Hastelloy B-3 reference are shown in Figure 1. The E_{corr} value for Pt was −6 mV. While Pt displayed reasonably low current density up to +1.0 V *vs* Hastelloy B-3, a transpassive breakdown was observed at +1.1 V. This behavior is unfavorable considering the required anodic potential for the reduction of UO_2 is ~2.5 V. An image of the platinum anode electrode after polarization is shown in Figure 2(a). The observed brownish coating formed on Pt after being subjected to anodic polarization in LiCl-Li_2O has been reported to be Li_2PtO_3 by Jeong *et al.*[16] An SEM micrograph of the Pt wire, given in Figure 2(b), shows the morphology of the anode after it was subjected to the anodic polarization described above.

Following control experiments with platinum, alternative materials were subjected to the identical tests. The data obtained from the potentiodynamic polarization experiments of nickel based superalloys Inconel 600 and 718, austenitic stainless steel alloy 316, W, Ni, Mo, and Ti are shown in Figures 3(a) through (g). A polarization curve of Pt is included in the graph of each material for reference. The average corrosion potentials [E_{corr}] and the average current density recorded at +1 V *vs* Hastelloy B-3 obtained from these data are provided

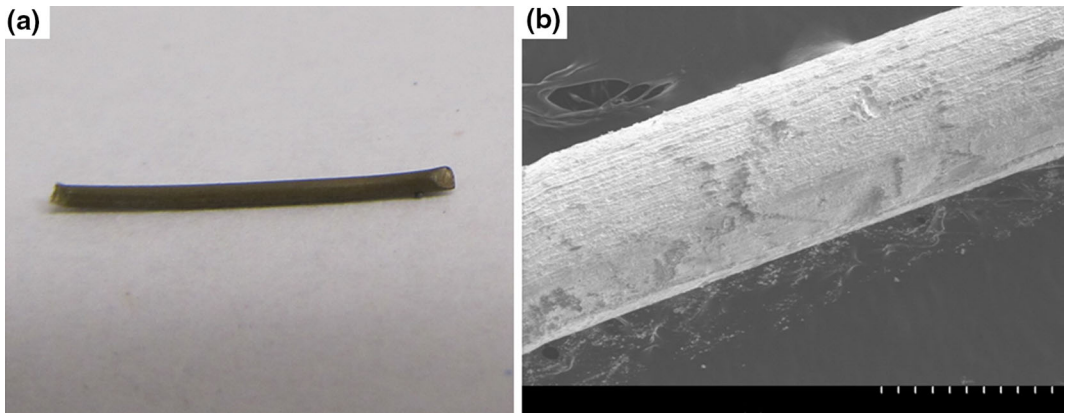

Fig. 2—Digital photograph (*a*) and an SEM micrograph (*b*) of platinum subjected to potentiodynamic polarization studies, the result of which was shown in Fig. 1. The scale bar in (b) represents 500 μm.

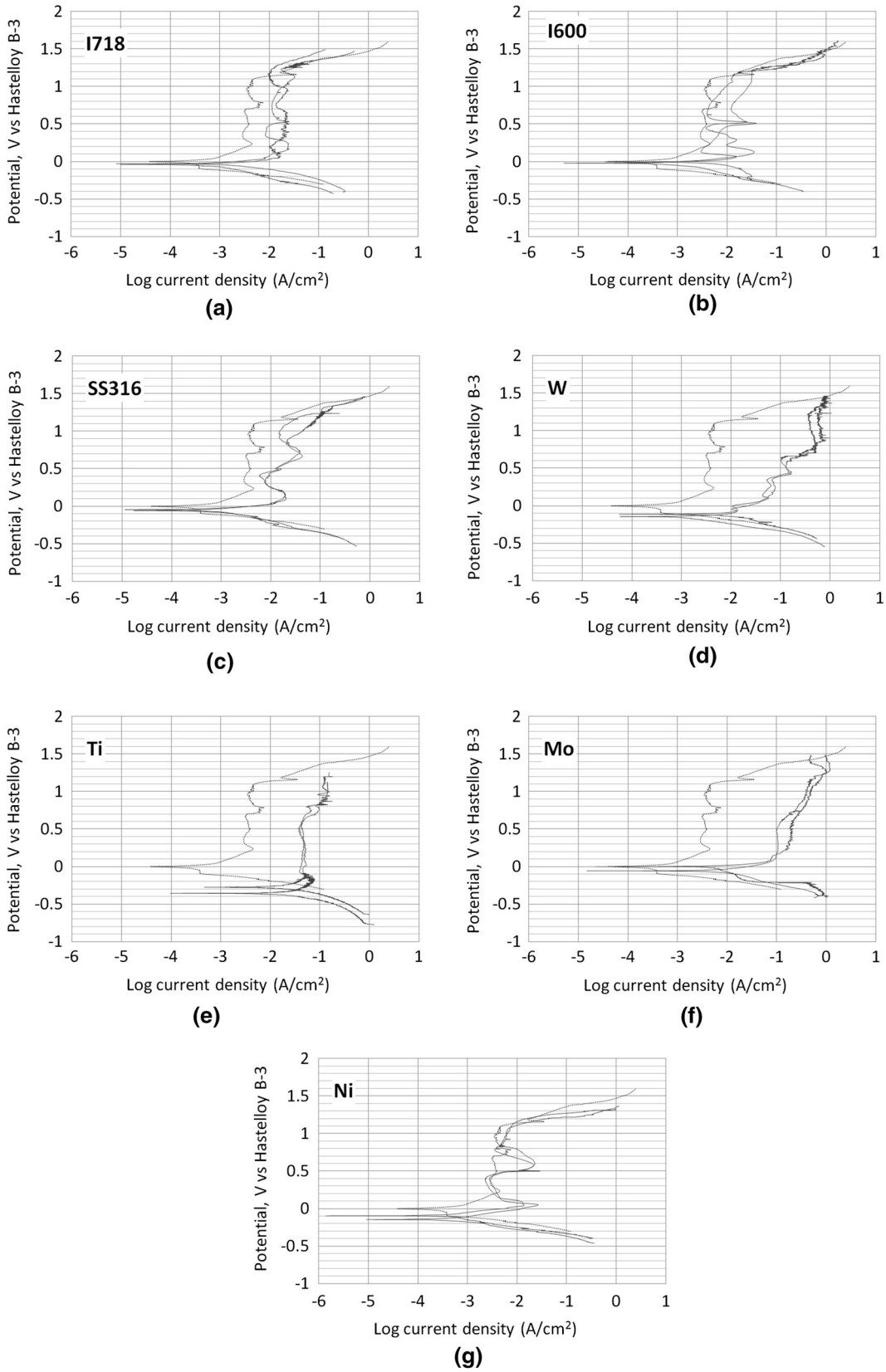

Fig. 3—Potentiodynamic polarization scans of (*a*) Inconel 718 (*b*) Inconel 600 (*c*) SS 316 (*d*) tungsten (*e*) titanium (*f*) molybdenum and (*g*) nickel measured against a Hastelloy B-3 reference in LiCl-2 wt pct Li_2O at 973 K (700 °C). The scans were performed at a rate of 1 mV/s. Duplicate scans are shown. A polarization scan of platinum recorded under the same conditions is shown as a dashed line for comparison.

Table II. Corrosion Potential (E_{corr}), Current Density Observed at +1 V *vs* Hastelloy B-3 and the Average Current Density Measured Across the Pseudo-Passive Region as Determined from the Potentiodynamic Polarization of Candidate Materials in LiCl-2 wt pct Li_2O at 973 K (700 °C)

Material	E_{corr} *vs* Hastelloy B-3 (mV)	Current Density at +1 V *vs* Hastelloy B-3 (A/cm^2)	Average Current Density Across the Passive/Pseudo-Passive/Constant Current Density Anodic Region (A/cm^2)
Pt	−6	1.4E-03	3.0E-03
Inconel 600	−22	9.3E-03	7.4E-03
Mo	−30	4.5E-01	2.5E-01
Inconel 718	−36	1.7E-02	1.5E-02
SS 316	−54	3.0E-02	2.0E-02
Ni	−121	6.2E-03	8.8E-03
W	−130	5.1E-01	2.4E-01
Ti	−317	1.4E-01	7.4E-02

Polarizations were conducted after the electrodes had been exposed to the salt for 60 s.

in Table II. While these average current densities can be indicative of behavior at a certain potential, the better metric would be the average current density over the entire passive/pseudo-passive/constant current density region. These values, also provided in Table II, show W to have one of the highest current densities in the anodic region. The implications of these results are discussed later.

Investigation of the polarization behavior revealed several differences between each metal. Mo exhibited the most noble E_{corr}; however, no passivation region was observed. The current density rapidly increased to greater than 100 mA/cm^2 within +100 mV above E_{corr}. The rise in current density resulted in extensive metal dissolution. Ti showed a similar lack of passivation behavior; however, the E_{corr} was extremely active at −316 mV *vs* Hastelloy B-3. As a result of its active potential, Ti would corrode significantly upon exposure to the electrolyte. Ni displayed promising passivation behavior, maintaining less than 30 mA/cm^2 of current density up to +1.2 V *vs* Hastelloy B-3. However, beyond this potential, the current quickly increased to 1 A/cm^2 and the anode underwent rapid corrosion. W exhibited a moderately active corrosion potential of −130 mV *vs* Hastelloy B-3. Anodic polarization of W produced lower current densities for the first +500 mV above E_{corr}, but current densities greater than 50 mA/cm^2 were observed beyond this potential region. While Mo exhibited the most noble E_{corr} of the metals investigated, only Ni exhibited a current density comparable to that of Pt at +1 V *vs* Hastelloy B-3. Moreover, W, Ti, and Mo exhibited current densities exceeding two orders of magnitude greater than the current density experienced by Pt at the same potential.

A remarkable trait of W was discovered after polarization. Compared to all other materials investigated, W appeared to be uniformly corroded at the end of the polarization experiment. The W electrodes exhibited a texture similar to that of an electropolished surface. The uniform surface of the tungsten electrode was unparalleled compared to other materials investigated in this study. This is a notable observation since the polarization of this electrode resulted in high current density. Furthermore, the uniformity of the corrosion of the W surface is a desirable trait for anode materials as it facilitates a constant surface potential during electrolysis. This observation prompted further investigations to study the corrosion characteristics of W and its mechanism of uniform oxidation when it is subjected to extremely high current densities at high potential required for reduction of UO_2.

Potentiodynamic polarization of nickel-based alloys showed slightly more active E_{corr} values than Pt, at −21.5 and −35.5 mV for Inconel 600 and 718, respectively. The polarization behavior of both alloys is predictably similar to Ni metal, especially in the case of Inconel 600 with 72 wt pct Ni. These two alloys exhibited similar transpassive breakdown behavior at roughly +1.2 V *vs* Hastelloy B-3. The Fe-Cr-Ni alloy, SS 316 also showed passivation behavior, however, not as pronounced as in the nickel-based alloys. Additionally, the SS 316 exhibited a lower transpassive breakdown potential of +0.9 V *vs* Hastelloy B-3. The current densities exhibited by the three alloys at +1 V *vs* Hastelloy B-3 only differed by a factor of three despite their significant differences in the alloy composition. Interestingly, these current densities are significantly greater than that of Pt and Ni at this potential and nearly an order of magnitude less than that of Mo, W, and Ti.

The results obtained through potentiodynamic polarization alone cannot be used to determine the ability of a material to be stable at the required anodic potential for the reduction of UO_2. In order to further investigate these materials at the required conditions, it was decided to examine three classifications of materials: a ferrous alloy, a nickel-based alloy, and a metal. Based on the above results and the recent reports,[18,22,26–28] Inconel 718, SS 316 and tungsten were selected for further investigations. Tungsten was specifically selected due to its previously demonstrated superiority over Ta, Pt, Hf, and Mo, quantified in terms of modulus of impedance and potential range of pseudo-passivation under anodic polarization in LiCl-Li_2O.[18,22] To determine the stability of the candidate anode materials under highly oxidizing conditions, the potential materials were polar-

ized at +2.5 V *vs* a SS 316 cathode in a two-electrode setup with LiCl-2 wt pct Li_2O as electrolyte. Electron microscopy was utilized following polarization to study the morphological changes that resulted from polarization. The micrographs obtained for these materials after being subjected to constant potential polarization in the molten salt are shown in Figures 4(a) through (c).

Microscopic analysis showed that SS 316 and Inconel 718 had undergone significant degradation as a result of polarization at +2.5 V *vs* SS316 in molten LiCl-2 wt pct Li_2O as shown in Figures 4(a) and (b), respectively. Both alloys suffered large morphological changes and crack formation. The nickel-based Inconel alloy experienced generalized corrosion and bulk material dissolution. The iron-based SS 316 underwent localized corrosion, and possibly cracking, which lead to significant material losses in localized regions. It is evident that neither alloy retained a consistent surface and would therefore not be reliable anodes for the electrolytic reduction of UO_2.

Surface morphology of the tungsten electrode subjected to constant potential polarization, shown in Figure 4(c), displayed superior structural stability compared to the alloys previously discussed. The anode retained no salt coating after rinsing, and structural degradation of the anode surface appeared minimal and was uniform. Of the three materials polarized to +2.5 V *vs* SS 316, W alone exhibited the desirable characteristic of uniform corrosion. As material surfaces oxidize and undergo corrosion, the ability to sustain electrolytic processes will be compromised as the electrode morphology and dimensions change leading to electrochemical potential changes. Therefore, tungsten's ability to maintain a stable surface throughout polarization is essential for it to function as an electrode in a large scale electrolytic reduction process.

To investigate the stability of tungsten in a wider range of electrolytes, W was polarized at +2.5 V *vs* SS316 in electrolytes containing varying amounts of Li_2O. A trend of increased anode corrosion with increasing Li_2O concentration in the electrolyte was observed as shown in Figures 4(c) and 5(a), (b). The average current density recorded during polarization in the three Li_2O concentrations differed by less than a factor of two; however, the amount of degradation experienced by the anodes exhibited a much stronger correlation to Li_2O concentration. The degradation of the anode surface is therefore likely from a separate chemical mechanism other than, or in addition to, increasing anodic current density.

To understand the surface chemistry of the W electrodes, the surfaces were studied using Raman spectroscopy. The regions from which spectra were obtained and the spectra of those surfaces are shown in Figures 6(a) through (c) and 7, respectively. Figure 6(a) of a W anode polarized in 2 wt pct Li_2O shows that the

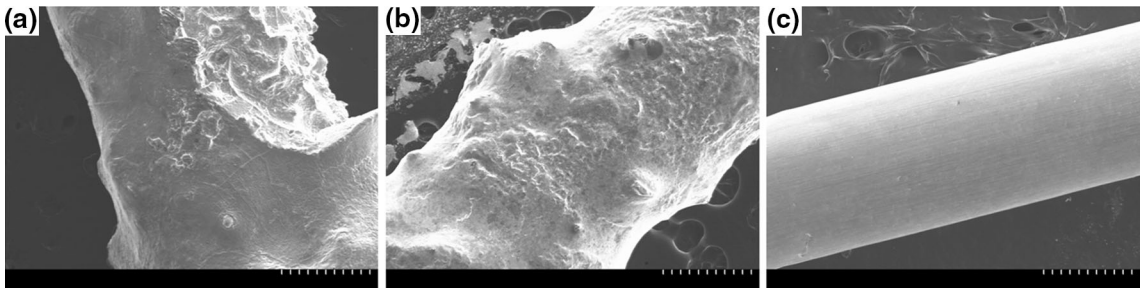

Fig. 4—Scanning electron micrographs of stainless steel alloy 316 (*a*), Inconel 718 (*b*) and tungsten (*c*) subjected to constant potential polarization at +2.5 V *vs* SS 316 for 600 s in LiCl-2 wt pct Li_2O at 973 K (700 °C). Of the three electrode materials, only W maintained the structural integrity. All scale bars represent 500 μm.

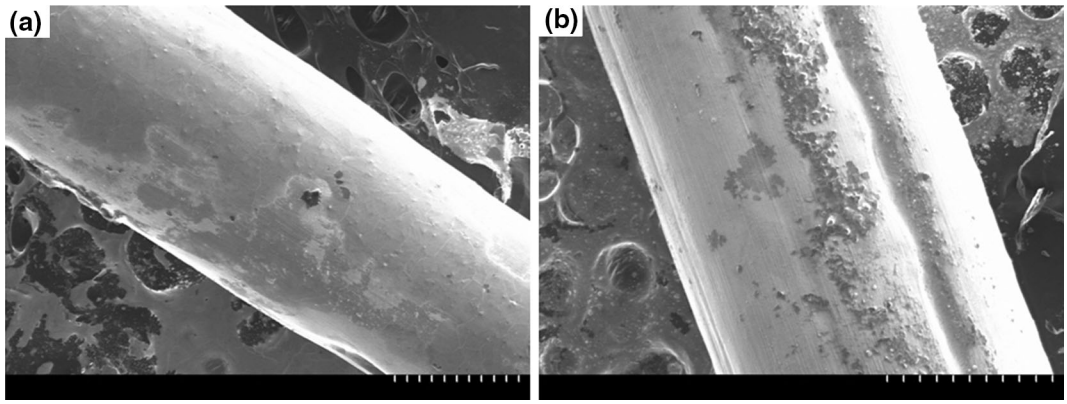

Fig. 5—Scanning electron micrographs of tungsten subjected to constant potential polarization at +2.5 V *vs* SS 316 for 600 s in LiCl-4 wt pct Li_2O (*a*) and LiCl-6 wt pct Li_2O (*b*) at 973 K (700 °C). Of the W electrodes exposed to LiCl containing varying concentrations of Li_2O, only the electrode exposed to LiCl containing 2 wt pct Li_2O (Fig. 5(c)) was found to result in a uniform surface. All scale bars represent 500 μm.

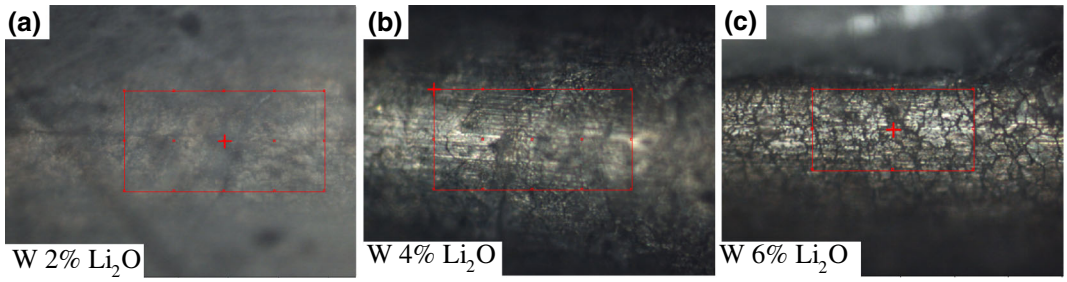

Fig. 6—Optical microscopy images of a W anode subjected to constant potential polarization +2.5 V *vs* SS 316 for 600 s in LiCl-2 wt pct Li_2O (*a*), 4 wt pct Li_2O (*b*), and 6 wt pct Li_2O (*c*). The imaging was performed at 100 times magnification. The red boxes indicate the regions from which the Raman Spectra shown in Fig. 8 were collected.

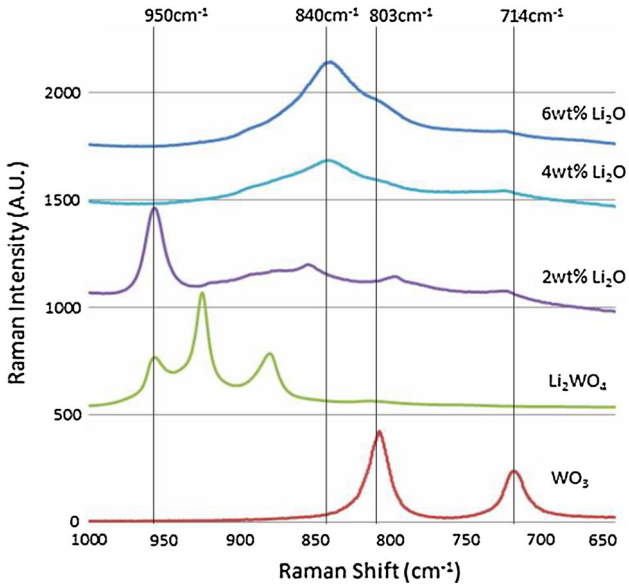

Fig. 7—Raman spectra averaged across W anode surfaces (shown in Fig. 7) subjected to constant potential polarization at +2.5 V *vs* SS 316 in LiCl with 2 wt pct Li_2O, 4 wt pct Li_2O, and 6 wt pct Li_2O, and compared to standard spectra of Li_2WO_4, and WO_3.

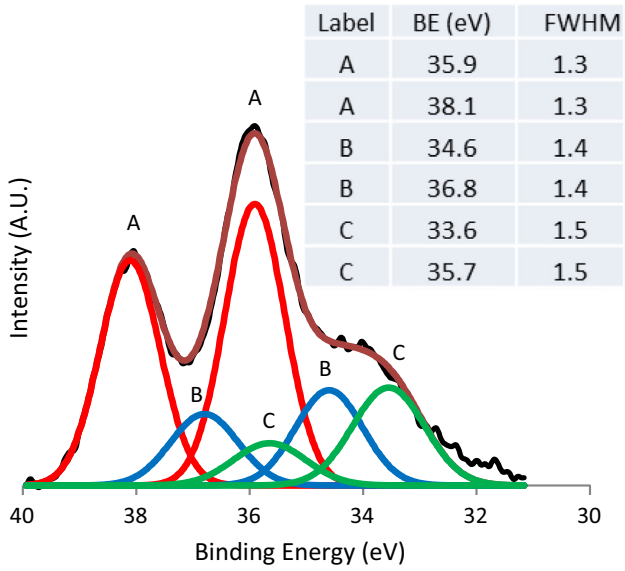

Fig. 8—Curve fitted W 4 f7 X-ray photoelectron spectrum of a W anode polarized at +2.5 V *vs* SS 316 in LiCl-2 wt pct Li_2O at 973 K (700 °C).

anode is completely encased in an opaque oxide film. The primary Raman vibrational mode of this film is at 950 cm^{-1} with minor features at approximately 850 and 790 cm^{-1}. The feature at 950 cm^{-1} is the vibrational mode of terminal W = O bonds and has been observed in Li^+-intercalated WO_3 (Li_xWO_3) films.[29–33] The Raman spectrum of Li_2WO_4, shown in Figure 7, contains terminal W = O bonds; however, the spectrum is dominated by the WO_4 stretching mode located at 930 cm^{-1}.[30,34] The lack of the primary W = O peak in the W anode spectra demonstrates that the W anodes did not form Li_2WO_4.

The W 4f7 and O 1s XPS spectra of a W anode polarized in LiCl-2 wt pct Li_2O are shown in Figures 8 and 9, respectively. The primary W 4f peak at 35.9 eV (peak A) is representative of W^{6+} in WO_3, while the two lower binding energy peaks at 34.6 eV and 33.6 eV (peaks B and C) arise from more reduced forms of W. Due to the non-stoichiometric nature of lithium-intercalated compounds, the valence state of the reduced forms of W cannot be determined. The O 1s spectrum also exhibits three separate bonding states with peaks at 531.9 eV (peak A), 530.6 eV (peak B), and 529.4 eV (peak C). Similar multi-valance oxygen spectra have been attributed to non-stoichiometric Li-intercalated Mo oxide compounds.[35] Significantly, Dupin *et al.* has reported W 4f7 and O 1s spectra of $Li_{0.35}WO_3$ with binding energies and full width half maximum values in excellent agreement with the anode spectra shown in Figures 8 and 9.[36]

The Li_xWO_3 surface film was not observable in the micrograph shown in Figure 4(c) because Li_xWO_3 compounds are hygroscopic and water soluble, and as a result, the film was dissolved during the electrode rinsing procedure prior to SEM studies. The film shown in Figure 6(a), from an un-rinsed electrode surface, completely covers the anode, forming an even surface barrier film between the W metal and the molten electrolyte. This analysis is complemented by the uniform surface observed in SEM analysis as the formation of such a film would result in an even oxidation rate across the electrode surface. The ability of W to undergo uniform corrosion when anodically polarized in LiCl-2 wt pct Li_2O is therefore attributed to the formation of a Li_xWO_3 oxide film.

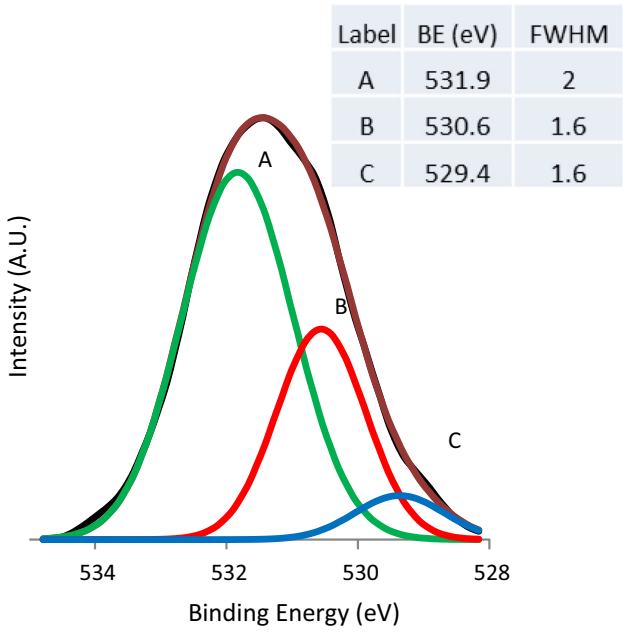

Fig. 9—Curve fitted O 1s X-ray photoelectron spectrum of a W anode polarized at +2.5 V *vs* SS 316 in LiCl-2 wt pct Li_2O at 973 K (700 °C).

Figure 6(b) shows that an incomplete surface film formed when W was subjected to polarization in 4 wt pct Li_2O. This film displays a different morphology than that formed in 2 wt pct Li_2O and is significantly less uniform. The Raman spectrum of this anode is shown in Figure 7 and display features at 840, 803, and 714 cm^{-1}. A standard spectrum of WO_3 shown in the same figure identifies the two shoulder features at 803 and 714 cm^{-1} as vibrational modes of WO_3. The primary feature at 840 cm^{-1} is the stretching mode of υ (O–O) complexes. Therefore, this peak is attributed to the evolution of O_2 gas on the anode surface and the formation of an intermediate peroxotungstate complex. Peroxotungstate complexes have been reported to demonstrate a primary Raman feature at 840 cm^{-1}.[37–39] Other vibrational modes observed in complex peroxotungstate compounds were not observed on the anode surface and as a result the exact molecular structure of the surface film cannot be identified.

As shown in Figure 6(c), the W anodes polarized in LiCl-6 wt pct Li_2O formed a severely cracked oxide film. The cracked nature of the surface film suggests that it is unstable and not protective. The Raman spectrum of this surface is characterized by the same peaks as the anode polarized in 4 wt pct Li_2O, but with greater intensity. The matching spectra indicate that the increase in Li_2O concentration, from 4 to 6 wt pct, enabled the formation of a peroxotungstate and WO_3 surface film that was not able to form at the lower concentration of Li_2O.

V. CONCLUSIONS

Potentiodynamic polarization experiments were conducted to study the stability of Inconel 600 and 718, stainless steel alloy 316, tungsten, nickel, molybdenum, and titanium in LiCl-2 wt pct Li_2O. Electrochemical techniques, combined with microscopy and spectroscopic analyses, were used to select the suitable candidate materials. Based on the results obtained from materials studied, it was determined that only tungsten possesses sufficient stability and exhibited uniform corrosion under highly anodic polarization in LiCl-2 wt pct Li_2O at 973 K (700 °C).

Oxidation of tungsten was studied at +2.5 V *vs* SS316 in LiCl at 973 K (700 °C) with varying concentrations of Li_2O to investigate the correlation between anode oxidation and the concentration of O^{2-} ions in the electrolyte. Raman and XPS spectroscopies showed that in LiCl-2 wt pct Li_2O, lithium-intercalated tungsten oxide formed a protective barrier film on the anode surface. This film was found to result in uniform oxidation of the W electrode. Higher concentrations of O^{2-} in the electrolyte lead to significant degradation of the anode due to the formation of an incomplete peroxotungstate and WO_3 oxide film on the surface. It is therefore suggested that tungsten be further studied as a potential anode material for the electrolytic reduction of UO_2 in LiCl containing at most 2 pct Li_2O.

VI. ACKNOWLEDGMENTS

This work was performed under the auspices of the US Nuclear Regulatory Commission (NRC) under contracts NRCHQ-11-G-38-0039 and NRC-38-10-949, and the Department of Energy (DOE) under Contract DE-FG30-08 CC0060. Ms. Nancy Hebron-Isreal serves as the grants program officer for the NRC awards and Mr. Gary Peterson served as the program manager for the DOE award.

ABBREVIATIONS

SS 316	Stainless steel alloy 316
SEM	Scanning electron microscope
E_{OCP}	Open circuit potential
E_{corr}	Corrosion potential
SHE	Standard hydrogen electrode

REFERENCES

1. J.J. Laidler, J.E. Battles, W.E. Miller, J.P. Ackerman, and E.L. Carls: *Prog. Nucl. Energy*, 1997, vol. 31, pp. 131–40.
2. J.P. Ackerman, T.R. Johnson, L.S.H. Chow, E.L. Carls, W.H. Hannum, and J.J. Laidler: *Prog. Nucl. Energy*, 1997, vol. 31, pp. 141–54.
3. S.W. Kwon, D.H. Ahn, E.H. Kim, and H.G. Ahn: *J. Ind. Eng. Chem.* (Seoul, Repub. Korea), 2009, vol. 15, pp. 86–91.
4. T. Inoue, T. Koyama, and Y. Arai: *Energy Proc.*, 2011, vol. 7, pp. 405–13.
5. S.M. Jeong, B.H. Park, J.-i.-m. Hur, C.-S. Seo, H. Lee, and K.-C. Song: *Nucl. Eng. Technol.*, 2010, vol. 42 pp. 183–92.
6. S. Herrmann, S. Li, and M. Simpson: *J. Nucl. Sci. Technol.*, 2007, vol. 44, pp. 361–67.
7. T. Shimada, N. Tedzuka, Y. Shimizu, and M. Miyake: *J. Alloys Compd.*, 1994, vol. 204, pp. 1–4.

8. M. Gibilaro, L. Cassayre, O. Lemoine, L. Massot, O. Dugne, R. Malmbeck, and P. Chamelot: *J. Nucl. Mater*., 2011, vol. 414, pp. 169–73.
9. Y. Sakamura: *J. Nucl. Mater*., 2011, vol. 412, pp. 177–83.
10. J.-M. Hur, C.-S. Seo, S.-S. Hong, D.-S. Kang, and S.-W. Park: *React. Kinet. Catal. Lett*., 2003, vol. 80, pp. 217–22.
11. D. Sri Maha Vishnu, N. Sanil, N. Murugesan, L. Shakila, C. Ramesh, K.S. Mohandas, and K. Nagarajan: *J. Nucl. Mater*., 2012, vol. 427 pp. 200–08.
12. B.H. Park, I.W. Lee, and C.S. Seo: *Chem. Eng. Sci*., 2008, vol. 63, pp. 3485–92.
13. R.Y. Liu, X. Wang, J.S. Zhang, and X.M. Wang: *J. Nucl. Mater*., 2004, vol. 327, pp. 194–201.
14. T. Usami, M. Kurata, T. Inoue, H.E. Sims, S.A. Beetham, and J.A. Jenkins: *J. Nucl. Mater*., 2002, vol. 300, pp. 15–26.
15. W. Park, J.-K. Kim, J.-M. Hur, E.-Y. Choi, H.S. Im, and S.-S. Hong: *J. Nucl. Mater*., 2013, vol. 432, pp. 175–81.
16. S.M. Jeong, H.-S. Shin, S.-H. Cho, J.-M. Hur, and H.S. Lee: *Electrochim. Acta*, 2009, vol. 54, pp. 6335–40.
17. F. Colom and A. de la Plaza: *J. Electroanal. Chem. Interfacial Electrochem*., 1990, vol. 290, pp. 105–18.
18. J. Ruppert, K.S. Raja, and M. Misra: in *Int. Congr. Adv. Nucl. Power Plants*, San Diego, 2010, pp. 1831–38.
19. J.-M. Hur, S.M. Jeong, and H. Lee: *Electrochem. Commun*., 2010, vol. 12, pp. 706–09.
20. M.K.Y. Sakamura and T. Inoue: *J. Electrochem. Soc*., 2006, vol. 153, pp. D31–39.
21. M. Iizuka, Y. Sakamura, and T. Inoue: *J. Nucl. Mater*., 2006, vol. 359, pp. 102–13.
22. M. Misra, K.S. Raja, and J. Ruppert: *ECS Trans*., 2010, vol. 33, pp. 181–92.
23. G. Inzelt: in *Handbook of Reference Electrodes*, G. Inzelt, A. Lewenstam, and F. Scholz, eds., Springer, Berlin Heidelberg, 2013, pp. 331-32.
24. T.B. Joseph, N. Sanil, L. Shakila, K.S. Mohandas, and K. Nagarajan: *Electrochim. Acta*, 2014, vol. 139, pp. 394–400.
25. S.A. Kuznetsov and M. Gaune-Escard: *J. Nucl. Mater*., 2009, vol. 389, pp. 108–14.
26. J. Indacochea and J. Smith: *J. Mater. Res*., 1999, vol. 14, pp. 1990–95.
27. A. Ravi Shankar, S. Mathiya, K. Thyagarajan, and U. Kamachi Mudali: *Metall. Mater. Trans. A*, 2010, vol. 41, pp. 1815–25.
28. S. Vandarkuzhali, N. Gogoi, S. Ghosh, B. Prabhakara Reddy, and K. Nagarajan: *Electrochim. Acta*, 2012, vol. 59, pp. 245–55.
29. U. Opara Krašovec, A. Šurca Vuk, and B. Orel: *Electrochim. Acta*, 2001, vol. 46, pp. 1921–29.
30. B.V.R. Chowdari, K.L. Tan, and W.T. Chia: *Solid State Ionics*, 53–56, 1992, vol. Part 2, pp. 1172–78.
31. C.G. Granqvist: *Handbook of Inorganic Electrochromic Materials*, Elsevier, Amsterdam, 2002.
32. S.-H. Lee, M.J. Seong, H.M. Cheong, E. Ozkan, E.C. Tracy, and S.K. Deb: *Solid State Ionics*, 2003, vol. 156, pp. 447–52.
33. T Kubo and Y Nishikitani: *J. Electrochem. Soc*., 1998, vol. 145, pp. 1729–34.
34. A.H. Ahmad and A.K. Arof: *Ionics*, 2004, vol. 10, pp. 200–05.
35. J. Świątowska-Mrowiecka, S. de Diesbach, V. Maurice, S. Zanna, L. Klein, E. Briand, I. Vickridge, and P. Marcus: *J. Phys. Chem. C*, 1058, vol. 112 (2008), pp. 11050–58.
36. J.C. Dupin, D. Gonbeau, I. Martin-Litas, P. Vinatier, and A. Levasseur: *J. Electron Spectrosc. Relat. Phenom*., 2001, vol. 120, pp. 55–65.
37. P. Delichere, P. Falaras,and A. Hugot-Le Goff: *Thin Solid Films*, 1988, vol. 161, pp. 47–58.
38. Z.P. Pai, D.I. Kochubey, P.V. Berdnikova, V.V. Kanazhevskiy, I.Y. Prikhod'ko, and Y.A Chesalov: *J. Mol. Catal. A: Chem*., 2010, vol. 332, pp. 122–27.
39. T.H.K. Kamata, S. Kuzua, and N. Mizuno: *J. Am. Chem. Soc*., 2009, vol. 131, pp. 6997–7004.